Pulse Characterization of Passively Mode-Locked Quantum-Dot Lasers Using a Delay Differential Equation Model Seeded With Measured Parameters

Ravi Raghunathan, Mark Thomas Crowley, Frédéric Grillot, *Senior Member, IEEE*, Yan Li, Jesse K. Mee, *Student Member, IEEE*, Vassilios Kovanis, and Luke F. Lester, *Fellow, IEEE*

***Abstract*—A delay differential equation-based model for passive mode locking in semiconductor lasers is shown to offer a powerful and versatile mathematical framework to simulate quantum-dot lasers, thereby offering an invaluable theoretical tool to study and comprehend the experimentally observed trends specific to such systems. To this end, mathematical relations are derived to transform physically measured quantities from the gain and loss spectra of the quantum-dot material into input parameters to seed the model. In the process, a novel approach toward extracting the carrier relaxation ratio for the device from the measured spectra, which enables a viable alternative to conventional pump–probe techniques, is presented. The simulation results not only support previously observed experimental results, but also offer invaluable insight into the device output dynamics and pulse characteristics that might not be readily understood using standard techniques such as autocorrelation and frequency-resolved optical gating.**

***Index Terms*—Delay differential equations (DDEs), frequency-resolved optical gating (FROG), mode-locked semiconductor lasers, pulse asymmetry, quantum-dot lasers, semiconductor device modeling.**

I. Introduction

OVER the last decade, quantum-dot mode-locked lasers (QDMLLs) have generated considerable interest as promising alternatives to quantum well (QW) sources, owing to their demonstrably superior performance characteristics [1]–[4]. Much of this interest in QDMLLs arises from the fact that certain properties unique to QD systems, such as low linewidth enhancement factors and reduced values of unsaturated gain and absorption enable a considerably wider map of operational stability, compared to their bulk and QW counterparts [3]–[6]. This is important, because most target applications require stable pulse generation over variable operating conditions. For instance, typical operating environments such as data centers require components to be able to tolerate high temperatures accompanied by rapid and considerable heat generation within the system. Consequently, devices need to be engineered to be able to sustain stable output pulses over a range of operating conditions [7]–[9]. This, in turn, necessitates the need to not only map out the parameter space of the device over a range of possible operating conditions, but also to gain insight into the functional parameters that are unique to QD systems and modify the properties of the device, compared to QW-based devices. With this objective, although a considerable amount of effort has gone into developing robust analytical and numerical models to describe passive mode locking in semiconductor lasers (and even modified specifically for QDMLLs), the information available in the literature about the properties unique to QD structures that give them superior performance characteristics relative to QW structures, and how they can be accessed and exploited so as to optimize device performance, is rather scarce. This has led to the associated theoretical and experimental work following two distinct paths, with the former focusing on developing analytical/numerical models of varying degrees of complexity to describe specific physical processes/phenomena, while the latter typically relies on a process of iterative design through an extensive testing and characterization. On the theoretical side, as more physical effects and processes are incorporated into the analysis, the model grows in complexity and evolves to encompass a large parameter space. But while this added complexity might enable a better understanding of the underlying device physics and operation, the lack of access to realistic values of many of the associated parameters at various operating conditions severely hinders the process of practical device design/engineering through numerical simulation.

Our previous work involved first deriving a condition for the onset of stable mode locking in a QDMLL [7], and subsequently, studying the temperature stability of QDMLLs based on measured temperature-dependent gain and loss spectra, where the gain and loss spectra were extracted as a function of gain section current density and absorber bias voltage, over a range of temperatures from 20 °C to 70 °C [8].

Manuscript received August 1, 2012; revised October 20, 2012; accepted November 9, 2012. This work was supported in part by the Air Force Office of Scientific Research under Award FA9550-10-1-0276 and Award FA9550-10-1-0463, the National Science Foundation under Grant ECCS-0903448, the Defense Threat Reduction Agency under Grant DTRA01-03-D-0009-0026, and the Silicon Research Corporation under Contract SRC-2009-HJ-2000.

R. Raghunathan and L. F. Lester are with the Center for High Technology Materials, University of New Mexico, Albuquerque, NM 87106 USA (e-mail: raghunat@unm.edu; luke@chtm.unm.edu).

M. T. Crowley is with BinOptics Corporation, Ithaca, NY 14850 USA (e-mail: markthomasc80@gmail.com).

F. Grillot is with Telecom Paristech, Ecole National Supérieure des Télécommunications, Centre National de la Recherche Scientifique Laboratoire Traitement et Communication de l' Information, 75634 Paris Cedex, France (e-mail: frederic.grillot@telecom-paristech.fr).

Y. Li is with APIC Corporation, Culver City, CA 90230 USA (e-mail: yanli@chtm.unm.edu).

J. K. Mee is with the Air Force Research Laboratory/RVSE, Kirtland Air Force Base, Albuquerque, NM 87117 USA (e-mail: Jesse.Mee@kirtland.af.mil).

V. Kovanis is with the Air Force Research Laboratory, Wright-Patterson Air Force Base, Dayton, OH 45433 USA (e-mail: vassilios.kovanis@wpafb.af.mil).

Color versions of one or more of the figures in this paper are available online at http://ieeexplore.ieee.org.

Digital Object Identifier 10.1109/JSTQE.2012.2230154

1077-260X/$31.00 © 2012 IEEE

In this paper, we present a systematic approach toward using a delay differential equation (DDE)-based model for passive mode locking in a semiconductor laser [10]–[13] as a powerful and versatile tool to simulate device behavior over a range of operating conditions and to potentially serve as a quantitative map to guide device design. Recent work has shown that variants of this model can be used to study phenomena such as injection locking [14], and a multisection version of the model has been recently developed to study passive mode locking [15], [16]. Relative to the other models used to study passive mode locking in semiconductor lasers, the DDE model has a parameter space of just nine parameters that can be mostly extracted from measurable physical quantities. Hence, we derive new expressions to transform experimentally measured quantities to model parameters, such as the carrier relaxation ratio of a QDMLL. The standard technique to determine this parameter, which is defined as the ratio of the gain relaxation rate to the absorber relaxation rate, involves measuring gain and absorber recovery times using pump–probe techniques, individually for the semiconductor optical amplifier [17] corresponding to the gain section, and for the saturable absorber [18], [19] corresponding to the absorber section of the two-section laser. The approach discussed in this study provides an analytical expression for the carrier relaxation ratio as a function of static parameters that can be easily measured on a multisection QD laser test structure over temperature, current density, bias voltage, and wavelength. This allows mapping out the carrier relaxation ratio of the QDMLL over a range of operating conditions, each of which can be used as an input parameter in the DDE model in order to simulate device performance at that condition, while circumventing the need to perform pump–probe measurements.

In using the DDE model in its original form, we find that the important operational characteristics of the device under study are captured without the need for additional equations or parameters, thereby preserving its relatively simple formalism. For example, our analysis is shown to simulate experimental trends accurately, without the need to include additional equations/transitions specific to dot energy levels in the model. Thus, the simulations accurately predict commonly observed experimental phenomena, such as pulse narrowing with increasing absorber bias. In addition, it will be shown that the simulations enable novel insight into properties unique to QD systems, such as the lower values of unsaturated gain and absorption compared to the corresponding values for QW devices, key trends in the behavior of the linewidth enhancement factor close to threshold in QD devices, and pulse asymmetry switching as a function of absorber bias. The last of these is an important dynamical effect, and, as will be shown, the close agreement between simulation results and experiment highlights the importance of the DDE model as an excellent theoretical tool to study dynamical trends in semiconductor lasers [20], [21].

The paper is organized as follows. In Section II, a new set of equations is derived using the definitions in [11] to transform experimentally measured data into dimensionless model parameters. After a brief description of the device structure, Section III uses the expressions derived in Section II to transform measured parameters for each set of operating conditions to seed the model and discusses the simulation results obtained. The simulation results are used to first verify well-established phenomena such as pulse trimming with increasing absorber bias. Next, they are shown to offer an indispensible theoretical tool to enable novel insight into experimental trends observed with diagnostic techniques such as autocorrelation and frequency-resolved optical gating (FROG). Conclusions are given in Section IV.

II. Transforming Experimental Data to Dimensionless Model Parameters

The DDE model due to Vladimirov and Turaev is derived from the coupled partial differential equation (PDE) formalism that describes the interaction of a slowly varying complex optical field with the carrier densities in the gain and absorber sections of a semiconductor laser, where parameters are generally functions of position and time [11], [12]

$$\frac{\partial E\left(t,z\right)}{\partial z}+\frac{1}{v}\frac{\partial E\left(t,z\right)}{\partial t}=\frac{g_r\Gamma_r}{2}\left(1-i\alpha_r\right)\left[N_r\left(t,z\right)-N_r^{tr}\right]E\left(t,z\right) \quad (1)$$

$$\frac{\partial N_r\left(t,z\right)}{\partial t}=J_r-\gamma_r N_r\left(t,z\right)-vg_r\Gamma_r\left[N_r\left(t,z\right)-N_r^{tr}\right]\left|E\left(t,z\right)\right|^2. \quad (2)$$

In (1) and (2) aforesaid, the subscript $r=g(r=q)$ corresponds to the gain (absorber) section. $E\left(t,z\right)$ describes the optical field in the two sections. The variables $N_{g,q}\left(t,z\right)$ denote carrier densities in the gain/absorber sections, while the variables $N_{g,q}^{\mathrm{tr}}$ are the carrier densities at transparency in the corresponding section. The parameter v is the light group velocity, assumed constant and equal in both sections. The parameters $\alpha_{g,q}, g_{g,q}, \Gamma_{g,q}$, and $\gamma_{g,q}$ are, respectively, the linewidth enhancement factors, differential gains, transverse modal fill factors, and carrier density relaxation rates in the gain and absorber sections. The parameters J_g and $J_q\,(=0)$ denote the injection current densities in the gain and absorber sections, respectively.

If a transformation is now performed to a frame of reference moving with the propagating pulse, the 2-D (spatiotemporal) system of PDEs is simplified to a 1-D (temporal) system of DDEs [11], [12]

$$\frac{dA\left(\tau\right)}{d\tau}=\gamma\sqrt{\kappa}\,\exp\left[\frac{1}{2}\{(1-i\alpha_g)G(\tau-T)-(1-i\alpha_q)Q(\tau-T)\}\right]A\left(\tau-T\right)-\gamma A\left(\tau\right) \quad (3)$$

$$\frac{dG\left(\tau\right)}{d\tau}=g_0-\Gamma G\left(\tau\right)-e^{-Q(\tau)}\left(e^{G(\tau)}-1\right)\left|A\left(\tau\right)\right|^2 \quad (4)$$

$$\frac{dQ\left(\tau\right)}{d\tau}=q_0-Q\left(\tau\right)-s\left(1-e^{-Q(\tau)}\right)\left|A\left(\tau\right)\right|^2. \quad (5)$$

In (3)–(5) previously, γ incorporates the effect of spectral filtering and ensures that a finite number of modes participate in the mode-locking process, α_g and α_q are the linewidth enhancement factors in the gain and absorber media, respectively, and κ accounts for linear cavity losses. The delay parameter incorporates history, which appears in the first equation of the model through the evaluation of optical field A, saturable gain G, and saturable loss Q at $\tau-T$, where T is the normalized

round trip time. The carrier relaxation ratio $\Gamma = (\tau_{\rm abs}/\tau_{\rm gain})$ is the ratio between the absorber and gain relaxation times, and s is the saturation parameter, defined as the ratio of the differential absorption to the differential gain. Finally, g_0 and q_0 are the unsaturated gain and absorption, respectively.

A recent experiment performed by our group [8] made use of the segmented contact method [22], [23] to obtain modal gain and total loss spectra as a function of current density, over absorber bias voltage and temperature for the QD material comprising the device. These curves were used to extract the modal gain $(g_{\rm mod})$ and unsaturated absorption (a_0) as a function of current density at each bias condition.

Now, from (2) in [8], we have the following threshold condition for lasing:

$$(g_{\rm mod}(J) - \alpha_i) L_g - (a_0 + \alpha_i) L_a = \alpha_m (L_a + L_g) \quad (6)$$

where, α_m and α_i represent, respectively, mirror losses and internal losses, and L_g and L_a represent, respectively, the gain and absorber section lengths, with

$$\alpha_m = \left(\frac{1}{L}\right) \ln\left(\frac{1}{\sqrt{R_1 R_2}}\right) \quad (7)$$

where $(L_g + L_a) = L$ and R_1, R_2 denote mirror reflectivities.

Substituting (7) into (6), we get

$$(g_{\rm mod}(J) - \alpha_i) L_g = (a_0 + \alpha_i) L_a - \left(\frac{1}{2}\right) \ln(R_1 R_2). \quad (8)$$

In the DDE model, G and Q describe the saturable gain and loss introduced by the gain and absorber sections, respectively, and $\kappa < 1$ describes the total roundtrip nonresonant linear intensity losses. Thus, the threshold condition for lasing is given by

$$\kappa e^{(G-Q)} = 1. \quad (9)$$

From (8) and (9), we find

$$G = (g_{\rm mod}(J) - \alpha_i) L_g \quad (10)$$

$$Q = (a_0 + \alpha_i) L_a \quad (11)$$

$$\kappa = \sqrt{R_1 R_2}. \quad (12)$$

Next, we derive expressions relating the saturable gain and loss (G and Q, respectively) to the unsaturated gain and absorption parameters (g_0 and q_0, respectively) from the definitions given in [11] (see the Appendix for complete derivations).

The following relations are obtained:

$$g_0 = \Gamma G \quad (13)$$

where $\Gamma = (\tau_{\rm abs}/\tau_{\rm gain})$.

Similarly

$$q_0 = (Q/s) \quad (14)$$

where

$$s \equiv \frac{g_q \Gamma_q}{g_g \Gamma_g} = \frac{[\partial g_{\rm mod}(J)/\partial J]_{g_{\rm mod}(J)=0}}{[\partial g_{\rm mod}(J)/\partial J]}. \quad (15)$$

It has previously been found that the differential gain at optical transparency, seen in the numerator, is a good estimate for g_q. We also make the reasonable assumption that the optical confinement factors in the gain and absorber sections are equal, so that $\Gamma_g = \Gamma_q$.

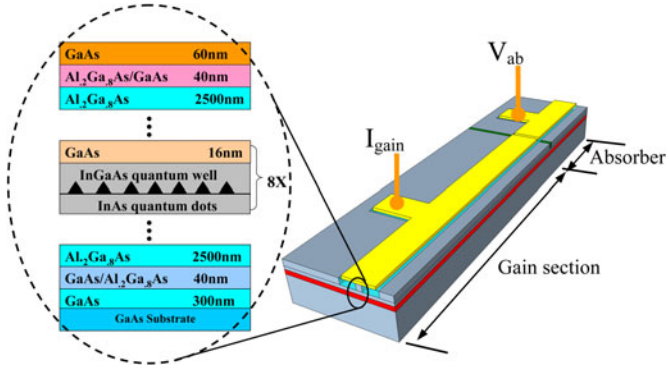

Fig. 1. Device schematic including details of epitaxial structure.

Further, in order to enforce the condition for stable, fundamental mode-locked operation (as opposed to Q switched, harmonic mode locked or continuous wave operation), we perform a linear stability analysis similar to that shown in [11] (Fig. 5), and arrive at the relation

$$q_0 = m g_0 \quad (16)$$

where m represents the slope of a line in the $g_0 - q_0$ plane, chosen to lie entirely within the region corresponding to the fundamental mode-locking regime. This yields an expression for the carrier relaxation ratio Γ which depends solely on measurable static device parameters defined previously in (10) and (11)

$$\Gamma = \left(\frac{Q}{mGs}\right) = \frac{(a_0 + \alpha_i) L_a}{m (g_{\rm mod}(J) - \alpha_i) L_g s}. \quad (17)$$

For the simulations in this paper, m was chosen to be 2. The carrier relaxation ratio of the device is, thus, extracted as a function of its measured modal gain and absorption parameters and its physical dimensions.

III. Results and Discussion

A. Description of Simulated Device

The device studied in this study is an 8-stack, dots-in-a-well (DWELL) laser structure grown by elemental source molecular beam epitaxy (MBE), with a 7-mm gain section and a 1-mm absorber section generating a 4.96-GHz pulse repetition rate under fundamental mode locking. A schematic of the device with important details of the epitaxial layer structure is shown in Fig. 1. The parameters appearing on the right-hand side of (17) can be readily measured as a function of gain-section current density, wavelength, absorber reverse bias and temperature using the segmented contact method [22], [23]. Previously, we used these measurables, namely, the gain and loss characteristics, to study the impact of temperature on the stability of QDMLLs [8].

B. Extraction of the Carrier Relaxation Ratio

The model parameter values used in determining Γ are summarized in Table I (-3-V absorber bias and device temperatures of 20 °C, 30 °C, 40 °C, 50 °C, and 60 °C) and represent values

TABLE I
MEASURED/EXTRACTED TEMPERATURE-DEPENDENT PARAMETER VALUES (DIMENSIONLESS) AT THE ONSET OF MODE LOCKING FOR A −3-V ABSORBER BIAS

T(°C)	G	Q	G-Q	Q/G	s	Γ
20	4.22	3.20	1.02	0.76	4.65	0.08
30	4.18	3.33	0.85	0.79	5.89	0.07
40	3.95	3.43	0.52	0.87	8.47	0.05
50	3.33	3.03	0.30	0.91	10.68	0.04
60	2.89	2.43	0.46	0.84	12.20	0.03

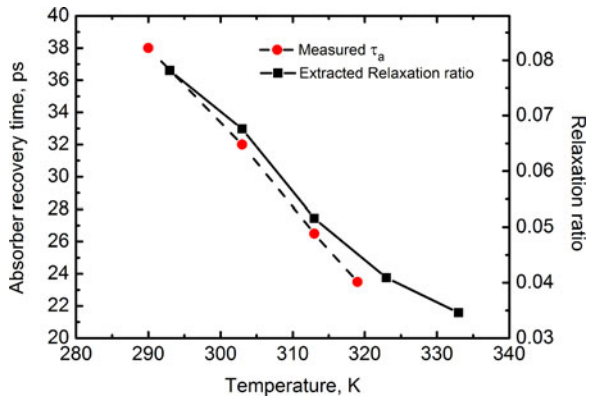

Fig. 2. Comparative plots of experimentally measured τ_a (solid circles) [19] and extracted relaxation ratio (solid squares) versus temperature.

at the onset of mode locking, i.e., the point at which a pulse was observed on an autocorrelator (AC) [8].

This data is plotted in Fig. 2 (solid squares), along with the values of absorption recovery times reported in [19] (solid circles) as a function of temperature. The similarity of the two plots suggests that the trend exhibited by (17) for Γ over temperature follows the trend exhibited by the absorption recovery time τ_a.

As a comparison, the pump–probe characterization of the absorber recovery times reported in [19] measured a decrease in the absorption recovery time with increasing temperature for a constant reverse bias of 2 V (the device studied in that work comprised a 190-nm active region, which corresponds to an electric field of 105 kV/cm). For a similar temperature range, with a 3-V reverse bias (288-nm active region, yielding an electric field of 104 kV/cm) and a similar QD epitaxial structure, we extract a comparable decrease in Γ, as seen from Fig. 2. While it is known that both gain and absorption recovery times decrease with temperature [19], [24], the similarity in the trends discussed earlier, together with the decreasing value of Γ in Table I is strongly suggestive that τ_a is the dominant factor in determining the behavior of Γ. Thus, it may be inferred that a decreasing value of Γ with increasing temperature suggests that the absorber recovery time decreases by a significantly larger factor than the corresponding reduction in the gain recovery time.

Table II shows the variation of the extracted relaxation ratio at a fixed temperature of 20 °C, for absorber bias voltages of 0, −3, and −5 V, wherein, a trend similar to that seen with increasing temperature is observed for Γ.

Again, the carrier relaxation ratio shows a decrease with increasing reverse bias. This trend agrees with the results obtained in [18] using pump–probe techniques, and supports the experimentally observed phenomenon that stronger bias voltages produce narrower pulses, given that pulse trimming is achieved primarily with faster absorption recovery rates, which shortens the net gain window during which pulses are generated.

TABLE II
MEASURED/EXTRACTED ABSORBER BIAS VOLTAGE-DEPENDENT PARAMETER VALUES (DIMENSIONLESS) AT THE ONSET OF MODE LOCKING AT 20 °C

V	G	Q	G-Q	Q/G	s	Γ
0	3.36	2.33	1.03	0.69	2.70	0.13
-3	4.22	3.20	1.02	0.76	4.65	0.08
-5	4.6	3.62	0.98	0.79	7.40	0.05

In view of the previous discussion, it can be seen that the trends exhibited by the carrier relaxation ratio Γ extracted from gain–loss data acquired by the segmented contact method using the expression derived previously in (17) follow the trends that can be expected by individually measuring τ_g and τ_a using pump–probe techniques, for a range of operating temperatures and bias voltages. Thus, it is reasonable to expect that this method of extracting Γ from gain and loss data provides a viable alternative to pump–probe measurements.

C. Transformation of Measured Values to Model Parameters

The expressions derived in Section II, particularly for the carrier relaxation ratio Γ, provide a convenient technique to accurately determine dimensionless parameters for input into the DDE model. Such a situation may be envisioned for a case where device performance needs to be simulated over a range of operating conditions.

A close examination of the system of DDEs given in (3)–(5) reveals the parameter space involved. Thus, in order to model a QDMLL realistically, it is imperative to constrain as many of the parameters as possible to values obtained from measurements on an actual QD device. The simulation results, obtained by seeding the model with these parameters (transformed to dimensionless form, using the relations derived in Section II), can then be used to interpret and characterize the mode-locking performance of the same device.

Since the onset of mode locking occurs at or beyond threshold, threshold values provide a convenient set of initial conditions for (3)–(5). The first step, then, is to use values measured at threshold in (10) and (11) to calculate $G(0)$ and $Q(0)$, and then use the values of $G(0)$ and $Q(0)$ in (13) and (14) to calculate the corresponding unsaturated parameters, g_0 and q_0, at threshold. Further, parameters κ and s can be directly found from (12) and (15), respectively, while the carrier relaxation ratio Γ is extracted from (17). Next, the absorber relaxation time is used to infer the delay parameter T and the spectral filtering coefficient γ for each operating condition as follows. The delay parameter T is calculated for each case by simply scaling the cavity round trip time to the absorber relaxation time for that case. In all cases, the absorber relaxation time was estimated from the experimental results in [18] and [19] for a saturable absorber with an epitaxial layer structure similar to the device simulated in this work, following from the discussion in the previous section. For instance, at an operating temperature of 20 °C, the bias voltage applied on the absorber section was expressed as an electric field strength across the active region. This value was then converted back to a bias voltage for the saturable absorber structure studied

TABLE III
SIMULATION PARAMETERS OVER BIAS VOLTAGE AT 20 °C

Parameter	0 V	–3 V	–5 V
T	3.23	5.00	6.67
G(0)	3.33	4.18	4.18
Q(0)	2.33	3.20	4.55
α_g	0.1	0.2	0.5
α_q	0.1	0.2	0.5
s	2.68	4.65	6.90
Γ	0.13	0.08	0.08
γ	29.14	39.15	41.10
κ	0.55	0.55	0.55

in [18], and the corresponding value of absorber relaxation time was found from [18] (Fig. 2). For higher temperatures, the exponential expression for thermionic emission given in [18] (eqn. (2)) was used to estimate the same. Also, the spectral filtering coefficient γ was estimated from the measured optical spectrum of the device as the product of the number of cavity modes taking part in the mode-locking process and the cavity intermode frequency spacing $\left(T^{-1}\right)$. Finally, the linewidth enhancement parameters in the gain and absorber sections were chosen such that the steady-state pulsewidth obtained from simulation was consistent with the typical pulsewidth measured on an AC for the actual device.

Now, having reduced the number of free parameters to two (namely, the linewidth enhancement factors in the gain and absorber sections), we set the two to be equal in order to simplify the analysis. Previous work [11], [25] has shown that this case corresponds to the most stable operating point, according to the DDE model. While this assumption could result in some departure from the actual values that the linewidth enhancement factors in the gain and absorber sections might take, the primary objective here is to study the broad trends, and how they might affect device performance. Further, it is reasonable to expect that any such departure may be marginal close to threshold, considering that the device under study in this study has a significantly longer gain section, so that the device behavior can be expected to be dominated by the gain section component. This value is then fit to the deconvolved AC pulsewidth measurement.

The results shown in the following were obtained as follows. The parameter values measured/extracted as discussed previously were used as initial conditions for the simulations. The system of equations defining the model (3), (4), and (5) was then integrated over two thousand round trip times, in order to enable the system to reach steady-state dynamics.

Table III lists the parameter values used to seed the simulations with parameters measured/extracted at saturable absorber bias conditions of 0, -3, and -5 V, at a temperature of 20 °C. As mentioned at the beginning of this section, the parameter values were obtained from the experimental data presented in [8], and made dimensionless for input into the model. The parameter values presented in Table III correspond to threshold conditions, i.e., current density values of 357 A/cm^2 at 0 V, 462 A/cm^2 at -3 V, and 537 A/cm^2 at -5 V (see ref: [8, Tables I and II]). As shown previously, the model is successful in capturing well-known trends in QDMLLs such as the effect of an increased absorber bias in trimming the pulses [26]. This paper discusses the mode-locking behavior and associated trends at an operating

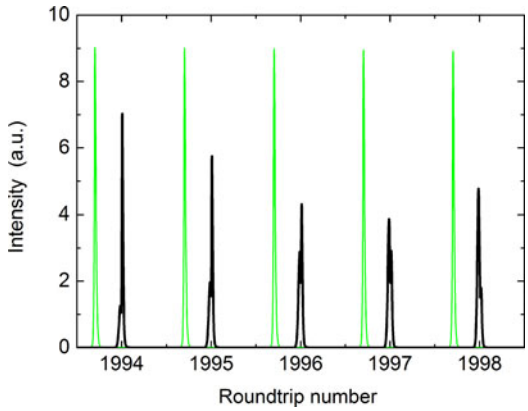

Fig. 3. Simulation results at 20 C and 5-V absorber reverse bias. Green pulse train is for $\alpha_{g,q} = 0.5$ and the black pulse train is for $\alpha_{g,q} = 1.2$, refer to Table IV.

temperature of 20 °C in more detail including the effect of the linewidth enhancement factor, by seeding the model with parameters extracted at three different absorber bias voltages, as detailed in Table III previously. As will be seen in Sections III-D and III-E in the following, the results predicted by simulation showed very good agreement with experimental observations.

One of the important predictive capabilities of the DDE model is the ability to gain insight into the range of values of the linewidth enhancement factor close to threshold for stable, fundamental mode-locking to be likely. It is seen that the linewidth enhancement factors in the gain and absorber sections have a profound influence on pulse structure, so that past a certain value of the linewidth enhancement factor, instabilities emerge in the pulse structure. Typical examples of instabilities of this type include pulse splitting and satellite pulses.

Consequently, sudden changes in pulse structure were used to determine mathematical ranges for the linewidth enhancement factor for stable, fundamental mode locking to be likely.

Table IV summarizes the mathematically likely ranges for α_g and α_q discussed previously, and the values used in each case to obtain a pulsewidth closest to what was obtained experimentally from AC measurements.

For instance, for the 5-V reverse bias case, the mathematically permissible range of α_g and α_q extends to 1.1, past which the structure of individual pulses exhibits instabilities such as splitting, as shown in Fig. 3 for $\alpha_{g,q} = 1.2$ (black pulse train), in sharp contrast to the stable pulses obtained with $\alpha_{g,q} = 0.5$ (green pulse train). As presented in Table IV, the general trend with increasing reverse bias is to reduce the range of acceptable linewidth enhancement factors for stable locking, although the device itself operates at a larger value with increasing reverse bias because of the consequent increase in threshold. Although a larger linewidth enhancement factor results in pulse broadening due to self-phase modulation, the improved pulse trimming at higher reverse bias in the absorber can help counteract this effect. The physics of these processes are all accounted for in the model.

D. DDE Simulations as an Indicator of Lower Unsaturated Gain and Absorption in QD Devices

Since the unsaturated gain and loss parameters are expected to be lower for QD structures in comparison to QW structures,

TABLE IV
LIKELY α-PARAMETER RANGES FOR STABLE, FUNDAMENTAL ML OVER BIAS VOLTAGE AT 20 °C

V	Range of α	$\alpha_g = \alpha_q$
0	$0 < \alpha_g = \alpha_q < 2.6$	0.1
-3	$0 < \alpha_g = \alpha_q < 2.1$	0.2
-5	$0 < \alpha_g = \alpha_q < 1.2$	0.5

TABLE V
COMPARISON OF PULSEWIDTHS (IN ps) OBTAINED EXPERIMENTALLY AND FROM SIMULATION RESULTS OVER BIAS VOLTAGE AT 20 °C

V	Autocorrelator τ_p	Actual τ_p [27]	DDE τ_p
0	25	16	16.25
-3	8	5.12	5

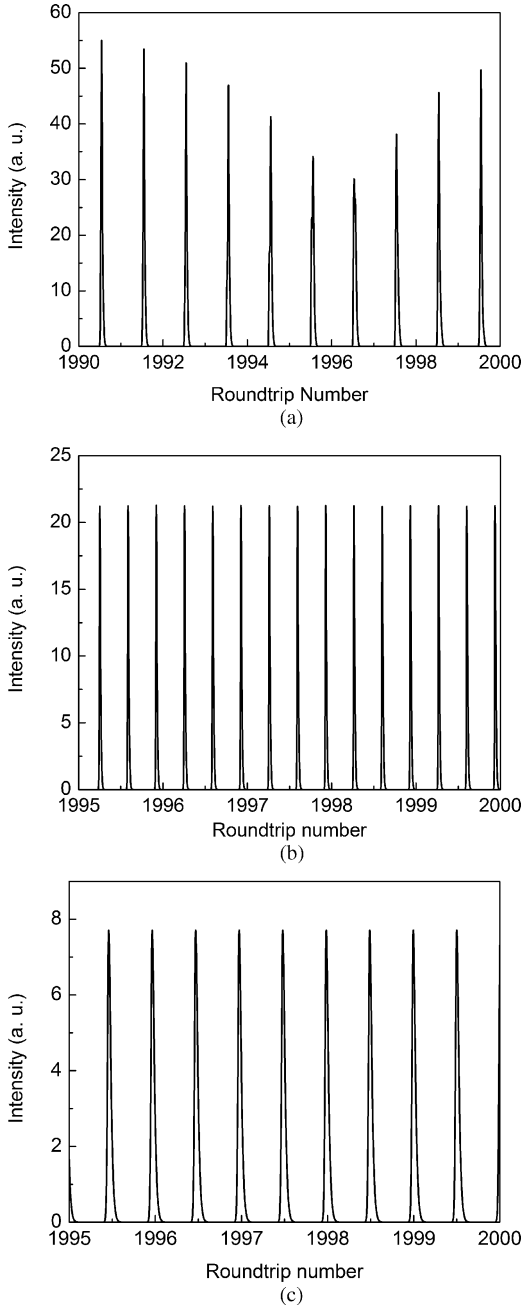

Fig. 4. (a) Simulation results at 20 C, 0-V absorber bias obtained with g_0 and q_0 increased tenfold (all other parameters as in Table III) show fluctuating intensities. (b) Simulation results at 20 C, -3-V absorber bias obtained with g_0 and q_0 increased fivefold (all other parameters as in Table III) show a transition to higher order mode locking. (c) Simulation results at 60 C, 0-V absorber bias obtained with g_0 and q_0 increased fivefold show a transition to higher order mode locking.

the effect of varying this pair of parameters was important to this study.

For an operating temperature of 20 °C and a 0 V reverse bias, the values of g_0 and q_0 can be extracted from the parameter values listed in the first column of Table III using (13) and (14). Next, keeping all other parameters unchanged from Table III, g_0 and q_0 are each scaled up by a factor of 10. As seen clearly from Fig. 4(a), this leads to significant instabilities in the steady-state output. Moreover, under the influence of an applied reverse bias on the absorber section or an elevated temperature [8], the simulation results predict stable, fundamental mode locking for an even smaller range of unsaturated gain and absorption.

For instance, for the cases $T = 20$ °C, -3-V bias [see Fig. 4(b)] and $T = 60$ °C, 0-V bias [see Fig. 4(c)], keeping all the parameter values unchanged, g_0 and q_0 were each scaled up by a factor of 5, whereby, the output is seen to have switched to higher order mode locking.

This suggests that even a fivefold increase in the values of g_0 and q_0 (which represents values typical of QW devices) is impractical for stable, fundamental mode locking for the QD device under study. This is strongly suggestive that in order for QD systems to achieve stable pulsation at the fundamental repetition rate at elevated temperatures or under an applied reverse bias, the values of unsaturated gain and absorption must be on the order of the values extracted in Tables I–III. Higher values tend to push the system out of the stable, fundamental mode-locking regime. In other words, the simulations show that lower values of unsaturated gain and absorption in the QD device under study compared to a QW version are necessary to achieve stable, fundamental mode locking.

Finally, Table V gives a comparison between typical pulsewidths obtained experimentally from AC measurements (assuming a sech^2-intensity profile [13]), and the corresponding values obtained by simulation using the DDE model. Comparing the last two columns shows very good agreement between the two.

However, to address subtleties in the DDE model regarding pulse shape, and not just width, a more complete characterization of the pulse is required. In the next section, FROG is used to measure the evolution of the pulse shape with increasing absorber bias and compared to the DDE model.

E. Correlation With FROG Measurements

The schematic diagram of the collinear second-harmonic generation (SHG) FROG system is shown in Fig. 5 [28]. The optical output of the laser is collected with an optical head, which integrates a lens, an isolator, and a short 1-m single-mode polarization-maintaining (PM) fiber pigtail, and then is coupled into the FROG system through a PM fiber. The

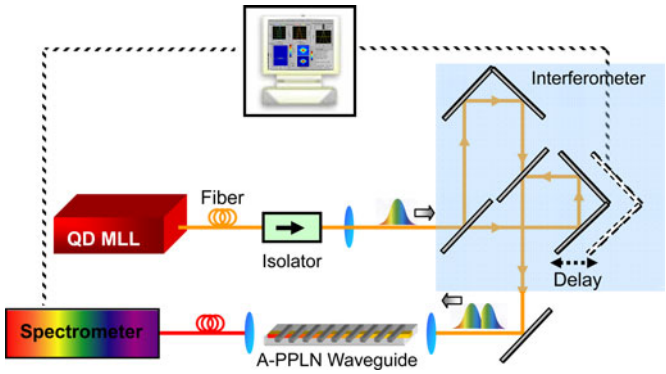

Fig. 5. Schematic diagram of the collinear SHG FROG system.

pulse train is sent into a free-space Michelson interferometer to produce pulse pairs with variable delay that are coupled into an aperiodically poled lithium niobate (A-PPLN) waveguide with a 6-cm long poling region to produce a SHG signal. The variable delay was produced by a voice coil-actuated servo having a delay resolution of 3.5 fs. The servo can be controlled either digitally via computer or by an analog waveform. The two delay pulses were sent collinearly into an A-PPLN waveguide.

The A-PPLN chip improves SHG conversion efficiency of the mode-locked diode lasers to a level that allows real-time data acquisition. By comparing the original QDMLL wavelength spectrum with the value computed from the FROG measurement, the bandwidth of the A-PPLN is verified to be sufficiently wide. At each relative time delay between the two pulse replicas, the SHG spectrum is recorded using an Ocean Optics QE65000 spectrometer. Because of the collinear geometry, interference fringes are produced. By applying an ac modulation to the servo position, the delay is modulated, and the fringes are averaged out if a sufficiently long integration time is used. The dc background from the low-pass filtered FROG trace is removed using background subtraction [29], [30]. The data acquisition, preprocessing, and processing were done using a commercial FROG software that was developed by Mesa Photonics.

FROG measurements on the device under study in this study revealed a curious trend. As seen from Fig. 6(a), a bias condition of a 95-mA gain current and a -3 V bias on the absorber section yielded a temporal pulse shape that is typical for such devices, with a steep rising edge, and a slower falling edge.

However, keeping the gain current fixed, when the absorber bias was increased to -5 V, the asymmetry of the pulse was observed to flip as seen in Fig. 6(b). Specifically, the trailing edge of the pulse is seen to show a faster decay than the rise time of the leading edge. An identical trend was seen at higher currents, such as the case shown in Fig. 6(c) and (d), where the pulse asymmetry reversal in going from an absorber bias of -3 to -5 V was observed for a gain current of 100 mA.

Simulation results of the DDE model seeded with physically measured parameters provide an invaluable tool to help understand this trend. Fig. 7 shows simulation results for the -5-V absorber bias condition near threshold at 20 °C, with $\alpha_g = \alpha_q = 1.1$ (solid green plots), and $\alpha_g = \alpha_q = 1.6$ (dashed red plots). The switching of pulse asymmetry can be clearly seen in Fig. 7(a), from the green, solid pulse, to the red, dashed pulse.

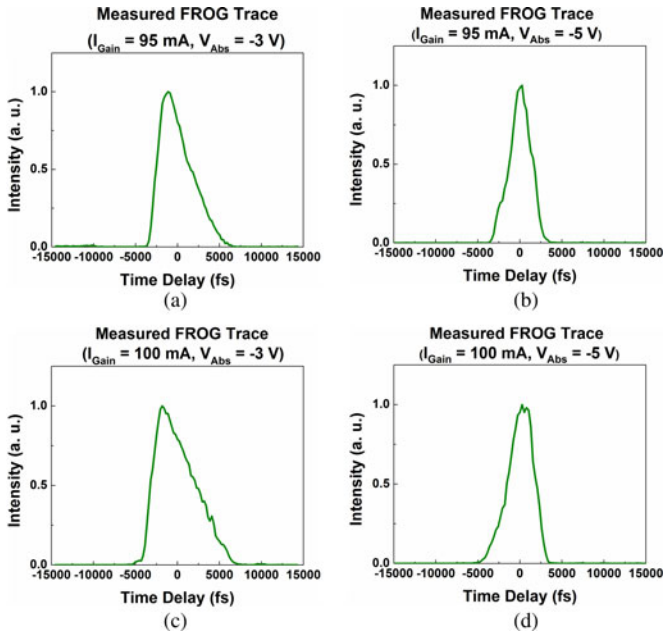

Fig. 6. Experimentally measured FROG traces showing the normalized temporal pulse intensity (clockwise from top left): (a) 95-mA gain current, -3-V absorber bias, (b) 95-mA gain current, -5-V absorber bias, (c) 100-mA gain current, -3-V absorber bias, and (d) 100-mA gain current, -5-V absorber bias.

The reversal in asymmetry may be interpreted as follows. At higher bias voltage, the gain section requires a higher threshold current, so that the higher concentration of injected carriers induces an increase in the linewidth enhancement factor. Combined with the length of the gain section, this results in significant pulse broadening due to dispersion and self-phase modulation as the pulse propagates through the gain section.

Simultaneously, the applied bias on the absorber section has the effect of expediting the sweep-out rate of the photogenerated carriers, leading to a faster recovery time. A careful comparison of the plots in Fig. 7(b) and (c) reveals the subtle distinguishing features between the two cases.

In the first case ($\alpha_g = \alpha_q = 1.1$, solid green curve), the pulse is "less broadened" in the gain section, owing to less self-phase modulation due to the relatively lower linewidth enhancement factor. Thus, the pulses exiting the gain section are expected to be narrower in the former case. The steeper leading (rising) edge associated with a narrower pulse causes the absorber to saturate rapidly, as seen from the green curves in Fig. 7(b).

By contrast, in the second case ($\alpha_g = \alpha_q = 1.6$, dashed red curve), a "more broadened" pulse exiting the gain section with a less steep leading edge profile is not able to saturate the absorber quite as fast, so that the absorber saturation is noticeably more gradual than in the former case, as seen from the dashed red curves in Fig. 7(b).

The trailing (falling) edge profile is governed by the absorber dynamics. On inspection of the saturable loss profiles shown in Fig. 7(b), one can observe that the absorber recovery is slightly more rapid for the dashed red plot ($\alpha_g = \alpha_q = 1.6$). Thus, due to the fact that the trailing edge experiences more loss at its tail, it is "better trimmed," so that the pulse has a steeper trailing (falling) edge. The combined effect of the gain and absorber sections is that in the former case ($\alpha_g = \alpha_q = 1.1$), the leading

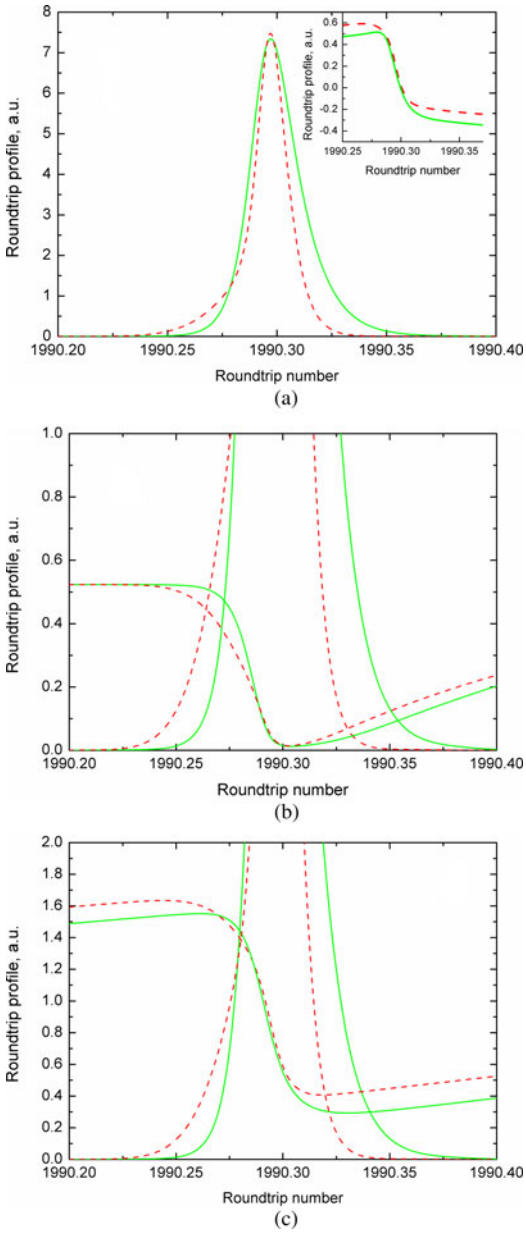

Fig. 7. Simulation results for the $T = 20\,^{\circ}\mathrm{C}$, $V_{abs} = -5$ V $\alpha_{g,q} = 1.1$ (solid green curves), $\alpha_{g,q} = 1.6$ (dashed red curves). (a) Temporal pulse profiles (inset shows corresponding net gain profiles), (b) shows the saturable loss profiles, and (c) shows the saturable gain profiles, superimposed on the temporal pulse profiles.

edge of the pulse is steeper, while the trailing edge shows a relatively gradual decay, whereas in the latter case ($\alpha_g = \alpha_q = 1.6$), the leading edge is less steep, the trailing edge is better trimmed, and the asymmetry is reversed.

Pulse asymmetry is a characteristic feature of mode-locked two-section quantum-dot lasers [31]. The variation of pulse asymmetry has been studied before in dye lasers [32], and simulated for a microchip laser system [33], and holds promise for applications such as chirp compensation and pulse compression. It is in such instances that simulation results of the DDE model seeded with measured parameters can provide an invaluable aid to complement the diagnostic techniques aforementioned.

IV. Conclusions

A (DDE) model for passive mode locking in semiconductor lasers, when seeded with QD laser-measured parameters, has been shown to accurately simulate experimental trends and observations. New expressions have been derived to transform quantities experimentally measured from gain and loss spectra to parameters suitable for input into the model. In particular, a novel approach for estimating the carrier relaxation ratio of a device from static gain and loss measurements has been discussed as a convenient alternative to conventional pump–probe techniques. The results of the simulations have been found to support experimental observations. The effect of increasing unsaturated gain and absorption, while retaining the values extracted from QD gain/loss measurements for the other parameters, was to predict departures from stable, fundamental mode locking in the output. Thus, it was shown that QDMLLs must operate with generally lower values of unsaturated gain and loss than QW devices. The simulations also predict a much lower range of values of linewidth enhancement factor for stable, fundamental mode locking to be probable, when a reverse bias is applied on the absorber section. In addition, the simulations yield information that is often not accessible from experimental techniques such as autocorrelation. Finally, the model provides invaluable insight into understanding abrupt transitions in the dynamics of the device output, such as the sudden switching of pulse asymmetry. This phenomenon was confirmed for the first time with direct FROG measurements of the laser.

Appendix

Following from (6)–(12) in Section II, here we derive expressions relating the saturable gain and loss (G and Q, respectively) to the unsaturated gain and absorption parameters (g_0 and q_0, respectively). From the definitions given in [11], we have (ζ and τ represent, respectively, spatial and temporal coordinates in the frame of reference of the pulse)

$$\begin{aligned} G(\tau) &= \int_{\zeta_3}^{\zeta_4} n_g(\tau,\zeta)d\zeta \\ &= \int_{\zeta_3}^{\zeta_4} \frac{v g_g \Gamma_g}{\gamma_q}\left[N_g(\tau,\zeta) - N_g^{tr}\right]d\zeta \qquad (1) \\ g_0 &= \int_{\zeta_3}^{\zeta_4} j_g d\zeta = \int_{\zeta_3}^{\zeta_4} \frac{v g_g \Gamma_g}{\gamma_q^2}\left(J_g - \gamma_g N_g^{tr}\right)d\zeta \end{aligned}$$

substituting for $J_g = \gamma_g \mathrm{N}_g$, we obtain

$$= \int_{\zeta_3}^{\zeta_4} \frac{v g_g \Gamma_g}{\gamma_q^2}\left[\gamma_g N_g(\tau,\zeta) - \gamma_g N_g^{tr}\right]d\zeta$$

$$\begin{aligned} g_0 &= \int_{\zeta_3}^{\zeta_4} \left(\frac{v g_g \Gamma_g}{\gamma_q}\right)\left(\frac{\gamma_g}{\gamma_q}\right)\left[N_g(\tau,\zeta) - N_g^{tr}\right]d\zeta \\ &= \Gamma \int_{\zeta_3}^{\zeta_4} \left(\frac{v g_g \Gamma_g}{\gamma_q}\right)\left[N_g(\tau,\zeta) - N_g^{tr}\right]d\zeta \qquad (2) \end{aligned}$$

where $\Gamma \equiv (\tau_q/\tau_g)$.

Comparing (1) and (2), we get

$$g_0 = \Gamma G. \qquad (3)$$

Similarly

$$Q(\tau) = -\int_{\zeta_2}^{\zeta_3} n_q(\tau,\zeta)d\zeta$$

$$= -\int_{\zeta_2}^{\zeta_3} \frac{vg_q\Gamma_q}{\gamma_q}\left[N_q(\tau,\zeta) - N_q^{tr}\right]d\zeta$$

$$Q(\tau) = -\int_{\zeta_2}^{\zeta_3} \frac{vg_q\Gamma_q}{\gamma_q^2}\left[\gamma_q N_q(\tau,\zeta) - \gamma_q N_q^{tr}\right]d\zeta$$

substituting for $\gamma_q N_q = J_q$, we obtain

$$= -\int_{\zeta_2}^{\zeta_3} \frac{vg_q\Gamma_q}{\gamma_q^2}\left[J_q(\tau,\zeta) - \gamma_q N_q^{tr}\right]d\zeta$$

$$Q(\tau) = \int_{\zeta_2}^{\zeta_3} \frac{vg_q\Gamma_q}{\gamma_q} N_q^{tr}d\zeta, \text{ since } J_q(\tau,\zeta) = 0$$

$$Q(\tau) = \int_{\zeta_2}^{\zeta_3} \left(\frac{v}{\gamma_q}\right)\left(\frac{g_q\Gamma_q}{g_g\Gamma_g}\right) g_g\Gamma_g N_q^{tr}d\zeta$$

$$= s\int_{\zeta_2}^{\zeta_3} \frac{vg_g\Gamma_g}{\gamma_q} N_q^{tr}d\zeta \tag{4}$$

where

$$s \equiv \frac{g_q\Gamma_q}{g_g\Gamma_g} = \frac{\left[\partial g_{\bmod}(J)/\partial J\right]_{g_{\bmod}(J)=0}}{\left[\partial g_{\bmod}(J)/\partial J\right]}. \tag{5}$$

Also

$$q_0 = \int_{\zeta_2}^{\zeta_3} j_q d\zeta = \int_{\zeta_2}^{\zeta_3} \frac{vg_g\Gamma_g}{\gamma_q} N_q^{tr}d\zeta. \tag{6}$$

Comparing (4) and (6), we get

$$q_0 = (Q/s). \tag{7}$$

Finally, we constrain the regime of operation to stable, fundamental mode locking using a dynamical stability analysis similar to that presented in [11] (Fig. 5). A suitable constraint to achieve stable, fundamental mode locking in terms of g_0 and q_0, is given by the locus of points lying on the line $q_0 = mg_0$, where m represents the slope of a line in the $g_0 - q_0$ plane, chosen to lie entirely within the region corresponding to the fundamental mode-locking regime.

Thus, we have, $\left(\frac{q_0}{g_0}\right) = m \Rightarrow \left(\frac{Q/s}{\Gamma G}\right) = m$. Therefore, using (10) and (11) from Section II, we obtain

$$\Gamma = \left(\frac{Q}{mG\,s}\right) = \frac{(a_0+\alpha_i)\,L_a}{m\,(g_{\bmod}(J)-\alpha_i)\,L_g s}. \tag{8}$$

ACKNOWLEDGMENTS

The authors would like to acknowledge insightful discussions with A. G. Vladimirov at the Weierstrass Institute, Berlin, Germany, concerning numerical simulations using the DDE model, and N. G. Usechak at the AFRL, Wright–Patterson Air Force Base, Dayton, OH, for valuable discussions relating to the use of the model for QDMLLs. The authors are also grateful to D. J. Kane of Mesa Photonics for guidance on FROG measurements and D. Chang, C. Langrock, and M. M. Fejer (all of the E. L. Ginzton Laboratory, Stanford University, Stanford, CA) for supplying the A-PPLN crystal for use in the FROG experimental setup. Vassilios Kovanis' work has been supported via the Electromagnetics Air Force Office of Scientific Research Portfolio of Arje Nachman.

REFERENCES

[1] M. T. Crowley, N. A. Naderi, H. Su, F. Grillot, and L. F. Lester, "GaAs-based quantum dot lasers in semiconductors and semimetals," in *Advances in Semiconductor Lasers,* vol. 86, New York: Academic, 2012, ch. 10.

[2] M. T. Crowley, V. Kovanis, and L. F. Lester, "Breakthroughs in semiconductor Lasers," *IEEE Photon. J.*, vol. 4, no. 2, pp. 565–569, Apr. 2012.

[3] E. U. Rafailov, M. A. Cataluna, and E. A. Avrutin, *Ultrafast Lasers Based on Quantum Dot Structures*. New York: Wiley, 2011.

[4] E. U. Rafailov, M. A. Cataluna, and W. Sibbett, "Mode-locked quantum-dot lasers," *Nat. Photon.*, vol. 1, pp. 395–401, 2007.

[5] M. G. Thompson, A. R. Rae, M. Xia, R. V. Penty, and I. H. White, "InGaAs quantum-dot mode-locked laser diodes," *IEEE J. Sel. Topics Quantum Electron.*, vol. 15, no. 3, pp. 661–672, May/Jun. 2009.

[6] G. T. Liu, A. Stintz, H. Li, K. J. Malloy, and L. F. Lester, "Extremely low room-temperature threshold current density diode lasers using InAs dots in $In_{0.15}Ga_{0.85}As$ quantum well," *Electron. Lett.*, vol. 35, pp. 1163–1165, 1999.

[7] C. Y. Lin, Y. C. Xin, Y. Li, F. L. Chiragh, and L.F. Lester, "Cavity design and characteristics of monolithic long-wavelength InAs/InP quantum dash passively mode-locked lasers," *Opt. Exp.*, vol. 17, pp. 19739–19748, 2009.

[8] M. T. Crowley, D. Murrell, N. Patel, M. Breivik, C. Y. Lin, Y. Li, B. O. Fimland, and L. F. Lester, "Analytical modeling of the temperature performance of monolithic passively mode–locked quantum dot lasers," *IEEE J. Quantum Electron.*, vol. 47, no. 8, pp. 1059–1068, Aug. 2011.

[9] J. K. Mee, M. T. Crowley, N. Patel, D. Murrell, R. Raghunathan, A. Aboketaf, A. Elshaari, S. F. Preble, P. Ampadu, and L. F. Lester, "A passively mode-locked quantum-dot laser operating over a broad temperature range," *Appl. Phys. Lett.*, vol. 101, no. 7, pp. 071112-1–071112-4, 2012.

[10] A. G. Vladimirov, D. Turaev, and G. Kozyreff, "Delay differential equations for mode–locked semiconductor lasers," *Opt. Lett.*, vol. 29, pp. 1221–1223, 2004.

[11] A. G. Vladimirov and D. Turaev, "Model for passive mode–locking in semiconductor lasers," *Phys. Rev. A*, vol. 72, pp. 033808-1–033808-13, 2005.

[12] A. G. Vladimirov and D. Turaev, "New model for mode–locking in semiconductor lasers," *Radiophys. Quantum Electron.*, vol. 47, pp. 769–776, 2004.

[13] N. G. Usechak, Y.-C. Xin, C.-Y. Lin, L. F. Lester, D. J. Kane, and V. Kovanis, "Modeling and direct electric field measurements of passively mode-locked quantum-dot lasers," *IEEE J. Sel. Topics Quantum Electron.*, vol. 15, no. 3, pp. 653–660, May/Jun. 2009.

[14] N. Rebrova, G. Huyet, D. Rachinskii, and A. G. Vladimirov, "Optically injected mode-locked laser," *Phys. Rev. E*, vol. 83, pp. 066202-1–066202-8, 2011.

[15] M. Rossetti, P. Bardella, and I. Montrosset, "Modeling passive mode-locking in quantum-dot lasers: A comparison between a finite-difference traveling-wave model and a delayed differential equation approach," *IEEE J. Quantum Electron.*, vol. 47, no. 5, pp. 569–576, May 2011.

[16] T. Xu, M. Rossetti, P. Bardella, and I. Montrosset, "Simulation and analysis of dynamic regimes involving ground and excited state transitions in quantum dot passively mode-locked lasers," *IEEE J. Quantum Electron.*, vol. 48, no. 9, pp. 1193–1202, Sep. 2012.

[17] Z. Bakonyi, H. Su, G. Onishchukov, L. F. Lester, A. L. Gray, T. C. Newell, and A. Tünnermann, "High–gain quantum–dot semiconductor optical amplifier for 1300 nm," *IEEE J. Quantum Electron.*, vol. 39, no. 11, pp. 1409–1414, Nov. 2003.

[18] D. B. Malins, A. Gomez–Iglesias, S. J. White, W. Sibbett, A. Miller, and E. U. Rafailov, "Ultrafast electroabsorption dynamics in an InAs quantum dot saturable absorber at 1.3 μm," *Appl. Phys. Lett.*, vol. 89, pp. 171111-1–171111-3, 2006.

[19] M. A. Cataluna, D. B. Malins, A. Gomez–Iglesias, W. Sibbett, A. Miller, and E. U. Rafailov, "Temperature dependence of electroabsorption dynamics in an InAs quantum–dot saturable absorber at 1.3 μm and its impact on mode–locked quantum–dot lasers," *Appl. Phys. Lett.*, vol. 97, pp. 121110-1–121110-3, 2010.

[20] T. Erneux, "Applied delay differential equations," in *Surveys and Tutorials in the Applied Mathematical Sciences*. vol. 3. New York: Springer, 2009.
[21] K. Ludge and H. G. Schuster, "Nonlinear laser dynamics," in *Annual Reviews of Nonlinear Dynamics and Complexity,* vol. 5, New York: Wiley, 2012.
[22] P. Blood, G. M. Lewis, P. M. Smowton, H. Summers, J. Thomson, and J. Lutti, "Characterization of semiconductor laser gain media by the segmented contact method," *IEEE J. Sel. Topics Quantum Electron.*, vol. 9, no. 5, pp. 1275–1282, Sep. 2003.
[23] Y. C. Xin, Y. Li, A. Martinez, T. J. Rotter, H. Su, L. Zhang, A. L. Gray, S. Luong, K. Sun, Z. Zou, J. Zilko, P. M. Varangis, and L. F. Lester, "Optical gain and absorption of quantum dots measured using an alternative segmented contact method," *IEEE J. Quantum Electron.*, vol. 42, no. 7, pp. 725–732, Jul. 2006.
[24] P. Borri, S. Schneider, W. Langbein, and D. Bimberg, "Ultrafast carrier dynamics in InGaAs quantum dot materials and devices," *J. Opt. A: Pure Appl. Opt.*, vol. 8, pp. S33–S46, 2006.
[25] A. G. Vladimirov, A. S. Pimenov, and D. Rachinskii, "Numerical study of dynamical regimes in a monolithic passively mode-locked semiconductor laser," *IEEE J. Quantum Electron.*, vol. 45, no. 5, pp. 462–468, May 2009.
[26] R. Raghunathan, M. T. Crowley, F. Grillot, S. D. Mukherjee, N. G. Usechak, V. Kovanis, and L. F. Lester, "Delay differential equation-based modeling of passively mode-locked quantum dot lasers using measured gain and loss spectra," in *Physics and Simulation of Optoelectronic Devices XX*. Bellingham, WA: SPIE, 2012.
[27] P. Vasil'ev, *Ultrafast Diode Lasers: Fundamentals and Applications*. Boston, MA: Artech House, 1995, p. 43.
[28] Y. Li, C.-Y. Lin, D. Chang, C. Langrock, M. M. Fejer, D. J. Kane, and L. F. Lester, "Pulse characterization of a passively mode-locked quantum dot semiconductor laser using FROG and autocorrelation," presented at the Conf. Lasers Electro Optics, Baltimore, MD, 2011.
[29] Ivan Amat-Roldán, Iain G. Cormack, and Pablo Loza-Alvarez, "Ultrashort pulse characterisation with SHG collinear-FROG," *Opt. Exp.*, vol. 12, pp. 1169–1178, 2004.
[30] S.-D Yang, A. M. Weiner, K. R. Parameswaran, and M. M. Fejer, "Ultrasensitive second-harmonic generation frequency-resolved optical gating by aperiodically poled $LiNbO_3$ waveguides at 1.5 μm," *Opt. Lett.*, vol. 30, no. 16, pp. 2164–2166, 2005.
[31] M. Radziunas, A. G. Vladimirov, E. A. Viktorov, G. Fiol, H. Schmeckebier, and D. Bimberg, "Strong pulse asymmetry in quantum-dot mode-locked semiconductor lasers," *Appl. Phys. Lett.*, vol. 98, pp. 031104-1–031104-3, 2011.
[32] A. Finch, G. Chen, W. Sleat, and W. Sibbett, "Pulse asymmetry in colliding pulse mode-locked dye laser," *J. Mod. Opt.*, vol. 35, pp. 345–354, 1988.
[33] G. Kozyreff, "Nonlinear aspects of the dynamics induced by dissipative light-matter interaction" Ph.D. dissertation, Brussels, Belgium, 2001.

Ravi Raghunathan received the Bachelor's of Applied Science (Hons.) degree in electrical engineering from the University of Windsor, Windsor, ON, Canada, in 2003, the Master's of Science degree in electrical engineering in electrophysics from the University of Southern California, Los Angeles, in 2006, and the Master's of Science degree in optical science and engineering from the University of New Mexico, Albuquerque, in 2010, where he is currently working toward the Ph.D. degree in optical science and engineering at the Center for High Technology Materials, University of New Mexico under the guidance of Prof. Luke F. Lester.

His current research interests include the theoretical and experimental investigation of various aspects of the device physics and characterization of semiconductor lasers, such as pulse compression and noise performance improvement in passively mode-locked quantum-dot lasers, ultrafast pulse characterization, nonlinear dynamical effects in semiconductor lasers, and the investigation of novel phenomena, such as nonlinear and quantum optical effects in semiconductor nanostructures.

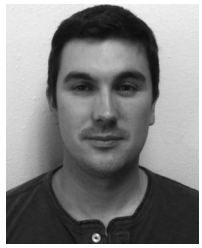

Mark Thomas Crowley received the B.Sc. (Hons.) degree in physics from University College Cork, Cork, Ireland, in 2004, and the Ph.D. degree in physics from Tyndall National Institute, University College Cork, in 2010, modeling electronic and optical properties of InGaAs/GaAs quantum dots under the supervision of Prof. Eoin O'Reilly. In 2004, he was an Intern with Prof. D. Cotter's Photonic Systems Group, University College Cork, researching four-wave mixing in highly nonlinear optical fibers.

Between 2010 and 2012, he was a Postdoctoral Researcher in Prof. Luke F. Lester's Group, Center for High Technology Materials, University of New Mexico. His postdoctoral work concentrated on the device physics, characterization, and modeling/design of semiconductor quantum-dot mode-locked lasers. He is currently a Design Engineer with BinOptics Corporation, Ithaca, NY.

Frédéric Grillot (SM'12) was born in Versailles, France, on August 22, 1974. He received the M.Sc. degree from the University of Dijon, Dijon, France, in 1999, the Ph.D. degree from the University of Besançon, Besançon, France, in 2003, and the Research Habilitation degree from the University of Paris VII, Paris, France, in 2012.

His doctoral research activities were conducted with the Optical Component Research Department, Alcatel-Lucent, involving research on the effects of optical feedback in semiconductor lasers, and the impact this phenomenon has on optical communication systems. He was with the Institut d'Electronique Fondamentale, University Paris-Sud, Orsay, France, from 2003 to 2004, where he was involved in research on integrated optics modeling and on Si-based passive devices for optical interconnects. From 2004 to 2012, he was working with the Institut National des Sciences Appliquées, Rennes, France, as an Assistant Professor. From 2008 to 2009, he was a Visiting Professor with the University of New Mexico, Albuquerque, where he was involved in research on optoelectronics with the Center for High Technology Materials. Since October 2012, he has been an Associate Professor within the Communications and Electronics Department, Telecom Paristech, Paris, France. He is a regular reviewer for several high-impact factor international journals. He is the author or coauthor of 41 journal papers, one book, two book chapters, and more than 70 contributions in international conferences. His current research interests include advanced laser diodes using new materials like quantum dots for low-cost applications and nonlinear dynamics in semiconductor lasers.

Dr. Grillot is a Senior Member of the International Society for Optical Engineers and of the IEEE Photonics Society as well as a regular member of the Optical Society of America.

Yan Li received the M.S. degree in optics from Sichuan University, Chengdu, China, in 2000, and the Ph.D. degree in optical science and engineering from the University of New Mexico, Albuquerque, in 2008.

His doctoral research work focused on high-speed modulation characteristics of quantum-dot lasers. He was a Senior R&D Engineer at Emcore Corporation in 2008. His main responsibility was to develop 10-Gb/s Transmit Optical Subassembly, Receiver Optical Subassembly, and liability improvement of 10-Gb/s VCSELs. From 2009 to 2011, he was a Postdoctoral Fellow in Prof. Luke F. Lester's Research Group, Center for High Technology Materials, University of New Mexico, focusing on modulation characteristics of high-speed quantum-dot (QD) semiconductor lasers, mode-locked QD lasers, and ultrafast pulse characterization. He is currently a Senior Processing Engineer at APIC Corporation, Culver City, CA, developing InP-based photonic integrated circuits. He has coauthored more than 30 journal publications and contributions to conferences.

Jesse K. Mee (S'10) received the B.S. degree in electrical engineering, concentrating on microelectronics and the M.S. degree (with the honor of distinction) in electrical engineering, in 2009 and 2010, respectively, both from the University of New Mexico, Albuquerque, where he is currently working toward the Ph.D. degree in optoelectronics at the Center for High Tech Materials under the guidance of Prof. Luke F. Lester.

His research was related to reliability physics of microelectronics for space applications. In particular, he concentrated on the reliability degradation phenomenon known as Negative Bias Temperature Instability. Since 2008, he has been with the Air Force Research Laboratories, Kirtland Air Force Base, Albuquerque, NM, and currently focuses on optical backplane design for satellite bus architecture. His research interests include high-temperature operation of passively mode-locked lasers, optical pulse compression, and integrated photonics.

Vassilios Kovanis studied physics at the University of Athens, Athens, Greece, followed by graduate work at Temple University, Philadelphia, PA. His Ph.D. dissertation at the University of New Mexico, Albuquerque, was focused on condensed matter theory.

He is a member of the technical staff and serves as a Lead Investigator Photonics Technologies Enterprise at the Sensors Directorate of the Air Force Research Laboratory (AFRL), Wright Patterson Air Force Base, Dayton, OH. His current responsibilities include managing an Air Force Office of Scientific Research Lab task on chip-scale next-generation laser radar for optical diverse waveform generation. He serves as a Defense Advanced Research Projects Agency agent for the Microsystems Technology, and Strategic Technology Offices in the areas of microwave photonics and transformational antenna programs. He is the lead Program Manager on the Optical Metamaterials AFRL/SENSORS Directorate enterprise. In September 1989, he joined the Nonlinear Optics Center at Air Force Weapons Laboratory, Kirtland Air Force Base, where for the next 11 years, he worked on multiple projects of optical and electronic technologies. Also during that period, he held research faculty positions with the Applied Mathematics and the Electrical Engineering Departments, University of New Mexico, and was a National Research Council Fellow between 1992 and 1994. Subsequently, he did a stint in corporate Research and Development Laboratories with Corning Inc., Corning, NY, as a Senior Research Scientist, managing technical interactions with telecommunications system houses and with BinOptics Corporation, Ithaca, NY, as a Program Manager, for next generation photonic product development. Between 2003 and 2005, he was a member of the faculty at the Applied Mathematics Department, Rochester Institute of Technology. He returned to AFRL in June of 2005. He has published extensively more than 80 referred and conference articles on issues of optical injection locking, coherence collapse, optical coupling of semiconductor lasers as well as in controlling, synchronizing, and communicating with chaotic waveforms, and has lectured in national and international settings. He maintains an h factor of 22 according to the Thomson Reuters (ISI) Web of Science citation index. He maintains an international research network of academics corporate, and defense scientists, including panel member of the NATO Metamaterials committee and a member of the U.S. Advanced Electronics Community of Interest.

Luke F. Lester (S'89–M'91–SM'01–F'13) received the B.S. degree in engineering physics and the Ph.D. degree in electrical engineering, in 1984 and 1992, respectively, both from Cornell University, Ithaca, NY.

He is a Professor and Interim Chair of the Department of Electrical and Computer Engineering and the Endowed Chair Professor in microelectronics at the University of New Mexico (UNM), Albuquerque. In August 2013, he will become the Department Head of the Bradley Electrical and Computer Engineering Department at Virginia Tech. Prior to joining UNM in 1994, he was an Engineer for the General Electric (Martin Marietta) Electronics Laboratory, Syracuse, NY, for six years where he worked on transistors for millimeter-wave applications. There in 1986 he coinvented the first pseudomorphic HEMT, a device that was later highlighted in the Guinness Book of World Records as the fastest transistor. In 1991, as a Ph.D. student in Prof. L. Eastman's Group, Cornell University, he researched and developed the first strained quantum-well lasers with millimeter-wave bandwidths. These lasers are now the industry standard for optical transmitters in data and telecommunications. In all, he has 27 years' experience in III–V semiconductor devices and advanced fabrication techniques. In 2001, he was a Co-Founder and Chief Technology Officer of Zia Laser, Inc., a startup company using quantum-dot laser technology to develop products for communications and computer/microprocessor applications. The company was later acquired by Innolume, GmbH. He has published more than 115 journal articles and more than 240 conference papers.

Dr. Lester is an active organizer and participant in the IEEE Photonics Society's conferences, workshops, and journals. He was a U.S. Air Force Summer Faculty Fellow in 2006 and 2007. His other awards and honors include a 1986 IEE *Electronics Letters* Premium Award for the first transistor amplifier at 94 GHz; the 1994 Martin Marietta Manager's Award; the Best Paper Award at SPIE's Photonics West 2000 for reporting a quantum-dot laser with the lowest semiconductor laser threshold; and the 2012 Harold E. Edgerton Award of the SPIE for his pioneering work on ultrafast quantum-dot mode-locked lasers.